THE MULTIMODE JAHN–TELLER EFFECT IN ONE–PHONON SIDE–BAND OF OPTICAL ABSORPTION SPECTRUM $\Gamma_8(^4A_2e^4t^3) \to \Gamma_8^{(\psi)}(^4T_1e^3t^4)$ OF THE CdTe:Co^{2+} SYSTEM

V. Z. Polinger[1], Yu. P. Gnatenko[1], P. N. Bukivsky[1], S. V. Melnichuk[2], I. M. Yurijchuk[2]
[1] *Institute of Physics, Nat. Ac. Sci. Ukraine, 46 Nauky Pr., Kiev-28, UA-252028, Ukraine*
[2] *Chernivtsi State University, 2 Kotsiubynskyi Str., Chernivtsi, UA-274012, Ukraine*

(Received August 27, 1997)

Complicated fine structure in the low–temperature optical absorption band of the impurity $d \to d$ transition $\Gamma_8(^4A_2e^4t^3) \to \Gamma_8^{(\psi)}(^4T_1e^3t^4)$ for semiconductor crystal CdTe doped by impurity Co^{2+} ions substituting tetrahedral Cd sites was studied experimentally and interpreted theoretically in terms of multimode Jahn–Teller effect for the excited term $\Gamma_8^{(\psi)}(^4T_1e^3t^4)$ coupled to trigonal and tetragonal modes. An attempt to use the old classical theory of impurity absorption ignoring the Jahn–Teller effect and treating the optical band in terms of phonon replicas turned out to fail. The one phonon side–band of the optical band in question has nothing in common with the projected phonon densities calculated for the defect crystal using the RIM–11 model. The multimode Jahn–Teller effect $\Gamma_8 \bigotimes (e + t_2)$ considered in terms of second–order perturbation theory resulted in a considerable redistribution of the projected densities of states and in appearance of new resonant vibronic modes. The experimental spectral line in the region of one–phonon side–band fitted well with the theoretical curve obtained by the adjustment of vibronic constants.

Key words: Jahn–Teller effect, optical absorption, phonon, vibronic spectrum

PACS numbers: 78.50.Ge

I. INTRODUCTION

Small–radius deep–level impurity electronic states belong to the most important characteristics of impurity crystals with partly filled d–shell substitutional impurity ions. These localized electronic states very often are degenerate due to a high symmetry crystal field of the nearest neighboring atoms. The inapplicability of adiabatic approximation (usually employed to separate nuclear motion from the electronic one) in the case of electronic degeneracy results in a complicated coupled motion of the impurity electrons and the lattice vibrational modes known as the Jahn–Teller effect [1,2].

Optical spectra of such a crystal give important information about the dynamic coupling of the impurity ion in question to the crystal matrix. At present the impurity spectroscopy has collected a considerable amount of experimental data on Jahn–Teller absorption and luminescence optical bands [2]. It is important to emphasise that a great majority of these works try to explain the experimental data in terms of the so–called cluster model. The main assumption of this model is that the Jahn–Teller impurity center together with a small number of its nearest–neighbor atoms involved in the degenerate electronic state may be considered as an isolated (or almost isolated) molecular group (a cluster), and instead of the infinite number of normal modes of the crystal the minimal number of normal vibrations of this separate group can be taken into account.

At the same time as is shown in [3] the cluster model can reproduce adequately the envelope of the broad optical bands only, the fine vibronic structure of the cluster–model optical band having no connection with the exact results. To reproduce correctly the fine vibronic structure one needs to take into consideration the multimode character of the vibronic coupling of degenerate impurity electronic states to normal modes of crystal lattice vibrations. In [4] all these problems are somehow got over and the theory is driven up to the numerical comparison with experimental data. This work concerns vibronic structure of one–phonon side–band in the luminescence spectrum $^2E(^2D) \to {}^2T_2(^2D)$ of the impurity system ZnS:Cu^{2+} with a strong Jahn–Teller coupling in both electronic terms participating in the electron transition.

In the present paper we consider the multimode Jahn–Teller effect in the excited electronic term $\Gamma_8^{(\psi)}(^4T_1e^3t^4)$ of the impurity–phonon system CdTe:Co^{2+} and its manifestations in a fine vibronic structure of the optical absorption band $\Gamma_8(^4A_2e^4t^3) \to \Gamma_8^{(\psi)}(^4T_1e^3t^4)$. It will be shown that in spite of the weak Jahn–Teller effect in this case the redetermination of spectral density resulting from the vibronic coupling is so essential that a fine structure of the optical band is impossible to be interpreted adequately without taking into consideration the Jahn–Teller effect.

Low temperature absorption spectra of the substituted impurity ion Co^{2+} in the semiconductor matrices $A^{II}B^{VI}$ have been considered in a series of papers among which the most important are Ryskin *et al.* [5], Natadze and Ryskin [6], Vasil'ev *et al.* [7], where the impurity system ZnS:Co^{2+} is investigated in detail, including a fine vibronic structure of optical absorption bands, the Jahn–Teller stabilization energy for the excited term $^4T_1(^4P)$ is estimated and the relative contribution in this energy from the vibronic coupling to trigonal and tetragonal vibrations is approximately calculated.

In section II of the present paper we present and discuss the experimental results on impurity absorption $^4A_2(^4F) \rightarrow {}^4T_1(^4P)$ in CdTe:Co^{2+}. In section III the crystal lattice dynamics of the impurity crystal CdTe:Co^{2+} is analyzed in terms of the rigid–ion model with 11 parameters, the defect of mass and of force constants being taken into consideration. In section IV the one–phonon side–band is presented as Fourier transform of a matrix correlation function which in its turn satisfies the known relations with the corresponding Green's function. The latter is found from the dynamic equations by the perturbation theory methods using the vibronic coupling constant as the small parameter of the theory. The resulting one–phonon side–band obtained theoretically is in satisfactory agreement with the experimental curve. The concluding section V is devoted to the discussion of the obtained results.

II. VIBRONIC STRUCTURE OF OPTICAL BANDS CORRESPONDING TO THE ELECTRONIC TRANSITION $^4A_2 \rightarrow {}^4T_1$ IN IMPURITY ABSORPTION SPECTRUM OF THE CdTe CRYSTAL DOPED WITH Co^{2+}

The impurity ions Co^{2+} in semiconductor crystal CdTe substitute cations, the Cd ions, and thereupon they are in tetrahedral surrounding of the four nearest neighboring Te ions. The ground electronic term of free Co^{2+} is ^4F. Under the crystal field of T_d symmetry it splits into three, $^4F = {}^4A_2 + {}^4T_1 + {}^4T_2$, the $^4A_2$ term being the ground one. Spin–orbit coupling transforms this term into the Kramers quadruplet Γ_8. The excited electronic term ^4P of free Co^{2+} under the tetrahedral crystal field transforms into $^4T_1$. The spin–orbit coupling splits $^4T_1$ into four, $^4T_1 = \Gamma_6 + \Gamma_7 + \Gamma_8^{(\varphi)} + \Gamma_8^{(\psi)}$ and in the first order perturbation theory with respect to spin–orbit interaction are accidentally degenerate. The corresponding energy level scheme of Co^{2+} in the tetrahedral crystal field with taking into account the spin–orbit coupling is given in fig. 1.

The energy gap separating the energy levels $^4A_2(^4F)$ and $^4T_1(^4P)$ for the ion Co^{2+} in the tetrahedral crystal field is $15B + 12Dq$, where B is the Racah parameter and Dq is the crystal field parameter. In the case under consideration $B = 485$ cm^{-1} and $Dq = 315$ cm^{-1}, i. e. the electronic transition $^4A_2 \rightarrow {}^4T_1$ should lie at about 11055 cm^{-1} ($\lambda = 8994$ Å), that is less than the forbidden zone energy gap of CdTe and therefore the corresponding impurity absorption gets into the transparency region of the crystal matrix.

The single crystals of CdTe have grown by the method of Bridgman. Concentration of the impurity ions Co^{2+} has been determined from the weight feed of ligature and constituted about $5 \cdot 10^{18} \div 10^{20}$ cm^{-1}. The absorption spectra measurements have been carried out with the spectrometer SDL–1. The spectral width of the monochromator gap did not exceed 1 cm^{-1}.

Fig. 2 presents the impurity absorption spectrum at

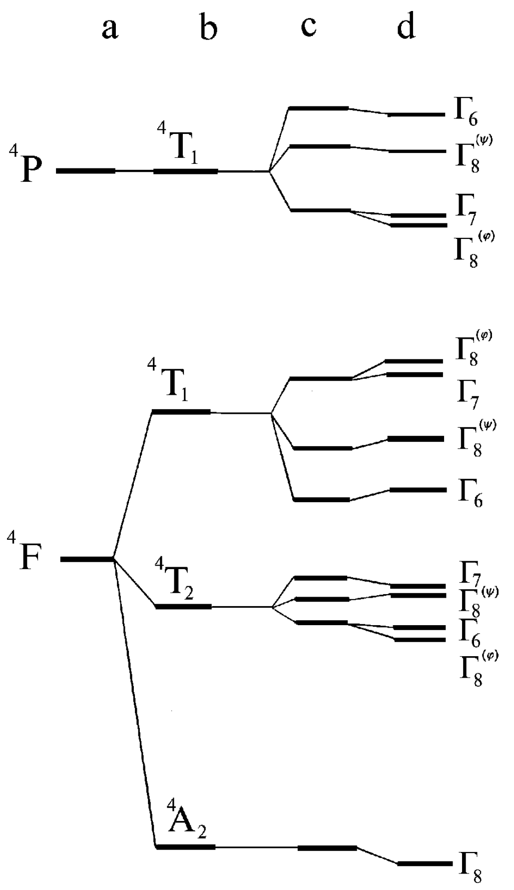

Fig. 1. The energy level scheme of Co^{2+} ion in tetrahedral crystal field of the nearest neighboring atoms in CdTe:Co^{2+} system: a) energy level of a free ion of Co^{2+}; b) crystal field splitting in the T_d symmetry case; c) effect of the first–order spin–orbit coupling **LS**; d) effect of the second–order spin–orbit coupling.

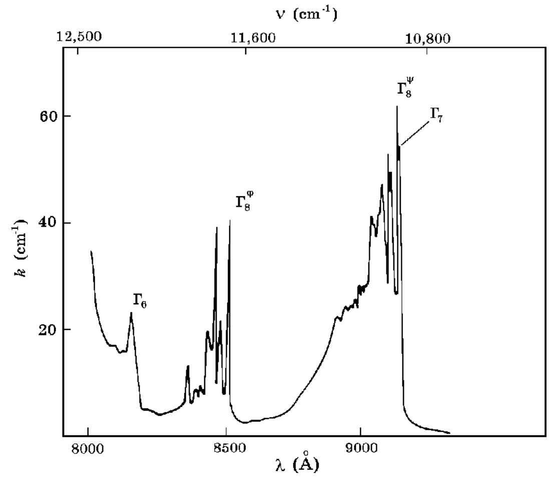

Fig. 2. The impurity absorption spectrum of CdTe:Co^{2+} crystals at $T = 4.2$ K in the spectral range of 10900 cm^{-1}–12300 cm^{-1} [$\Gamma_8(^4A_2) \rightarrow \Gamma_8^{(\psi)}(^4T_1)$ transition].

$T = 4.2$ K of the system in question CdTe:Co^{2+} in the spectral range 10900–12300 cm^{-1} which we attribute to the optical transitions to the spin–orbital components of the ${}^4T_1({}^4P)$ term. One can separate three comparatively narrow bands each beginning with an intensive line corresponding to zero–phonon transition from the ground $\Gamma_8({}^4A_2)$ term to the one of the spin–orbital components of the excited ${}^4T_1({}^4P)$ term. According to the energy level scheme presented in fig. 1 the long–range edge spectral lines correspond to the components Γ_7 and $\Gamma_8^{(\varphi)}$ accidentally degenerated in the first order perturbation theory with respect to spin–orbit interaction and slightly split in the second order. The long–wave lines of the two remaining optical bands can be attributed to transitions to the spin–orbital components $\Gamma_8^{(\psi)}$ and Γ_6 with the zero–phonon lines at 11769 cm^{-1} and 12275 cm^{-1} respectively. The spin–orbital Hamiltonian $\lambda\mathbf{LS}$ can be diagonalized by the well–known vector coupling scheme resulting in the following eigenvalues: $E(\Gamma_7) = E(\Gamma_8^{(\varphi)}) = 3\lambda/2$, $E(\Gamma_8^{(\psi)}) = -\lambda$ and $E(\Gamma_6) = -5\lambda/2$. Note that the interval rule $\{E(\Gamma_6) - E(\Gamma_8^{(\psi)})\} : \{E(\Gamma_8^{(\psi)}) - E(\Gamma_7)\} = 3 : 5$ is satisfied in the observed absorption spectrum and this makes us hope that the above assignment of the spectral lines is correct. The energy interval between the edge spin–orbital components equals 4 wherefrom comparing this result with the spectral position of the mentioned zero–phonon lines we find $\lambda = -330$ cm^{-1}. This value is about twice as large as the free–ion magnitude for Co^{2+}, $\lambda = -178$ cm^{-1}. This can be explained by the covalence effect with taking into account that the Te atom possesses a significantly larger value of spin–orbital coupling constant.

As seen from fig. 2 the optical bands corresponding to the transitions to the terms Γ_7 and $\Gamma_8^{(\varphi)}$ overlap and cannot be analyzed separately without taking into consideration the nonadiabatic mixing of these terms. To interpret theoretically this complicated mixed optical band the vibronic problem $\Gamma_7 + \Gamma_8^{(\varphi)} \bigotimes (e + t_2)$ should be solved, the problem of a combined Jahn–Teller and pseudo–Jahn–Teller effect for the close–in–energy degenerate electronic terms. This problem will not be considered in the present paper.

As distinguished from the term Γ_7 and $\Gamma_8^{(\varphi)}$ the electronic energy level $\Gamma_8^{(\psi)}$ is well separated from the other electronic terms and the corresponding optical absorption band at 11769 cm^{-1} does not overlap with the other bands. This circumstance allows to use the modified Born–Oppenheimer approximation [2] and to consider the degenerate electronic term $\Gamma_8^{(\psi)}$ separately and independently from the other electronic terms. The vibronic mixing of the four degenerate electronic states of the term $\Gamma_8^{(\psi)}$ causes the Jahn–Teller effect $\Gamma_8 \bigotimes (e + t_2)$ considered in detail in section IV. Note that though the ground electronic term $\Gamma_8({}^4A_2)$ in principle also can be coupled to e and t_2 vibrations, the corresponding vibronic coupling constants are negligibly small because they are non–equal to zero beginning from the second order in spin–orbit interaction for the orbital singlet ${}^4A_2$. Therefore, the Jahn–Teller effect for the ground $\Gamma_8({}^4A_2)$ term can be neglected and in this sense the optical transition ${}^4A_2 \to {}^4T_1$ is analogous to a simpler case of a singlet–quadruplet transition.

III. LOCAL DYNAMICS OF THE IMPURITY CRYSTAL LATTICE OF CdTe:Co^{2+}

The semiconductor crystals of the type $A^{II}B^{VI}$ are characterized by a mixed ionic–covalent type of chemical bonding. Therefore in this case a correct taking into account of the long–range and short–range forces simultaneously is very important. One of the well developed and widely used theoretical approaches for such crystals is the rigid ions model (RIM). Kunc [8] employed the RIM–11 (11 is the number of adjusting parameters) for a large series of semiconductor crystals of the type $A^{II}B^{VI}$ (for CdTe this was done by Plumelle and Vandevyver [9]) which resulted in the fitting of the phonon spectra calculated theoretically with the experimental data on the elastic neutron scattering.

All the details of the crystal lattice dynamics are obtained by a numerical diagonalization of the dynamic matrix of the harmonic crystal lattice in question at every point $\mathbf{k}$ of Brillouin zone resulting in eigenvalues $\omega_j(\mathbf{k})$ and eigenvectors $w_\alpha(j\mathbf{k})$ of this matrix (j — numbers branches of vibrational modes). In the RIM–11 the dynamic matrix is expressed in terms of 11 parameters their values taken from the constants of elasticity and energies of vibrational quanta of optical phonons at $\mathbf{k} = 0$ measured experimentally.

Doping the host crystal with substitutional impurities may result in the appearance of new vibrational frequencies in the allowed and (or) forbidden zones, the so–called resonant and local modes respectively. The appearance of resonant modes is accompanied with a considerable redistribution of projected densities of phonon states. We assume that the impurity doping effects can be described as a perturbation of the dynamic matrix of lattice vibrations, this perturbation being localized within the first coordination sphere of the impurity center. Thereupon these effects can be reduced to a defect of mass of the substituted ion and to a defect of force constants which correspond to the elastic interaction of the impurity ion to its nearest neighboring atoms. From the symmetry arguments it follows that in our case these force constants f are altered by the same value, and this alteration can be described by single parameter $t = (f - f')/f$ only.

Thus for the crystal CdTe of the zinc–blend type the impurity complex contains the impurity atom Co^{2+} together with the tetrahedrally coordinated four Te atoms of its nearest neighbor surrounding. The number of atoms in this complex equals five and the manifold of nuclear displacements under consideration is 15–fold dimension. Under the point symmetry group T_d of the impurity complex the 15–fold representation of nuclear displacements Γ_{tot} is decomposed into irreducible ones, $\Gamma_{tot} = A_1 + E + T_1 + 3T_2$.

To obtain the projected densities of states determining different irreducible contributions in the optical band one needs to relate the symmetrized nuclear displacements of the impurity complex $Q_{\mu\Gamma\gamma}$ transforming after the row γ of irreducible representation Γ to normal modes of the crystal lattice vibrations $Q(j\mathbf{k})$:

$$Q_{\mu\Gamma\gamma} = \sum_{æ} a_{æ}(\mu\Gamma\gamma) Q_{æ}. \qquad (1)$$

Hereafter instead of $\mathbf{k}$ and j we use the combined index $æ = \{\mathbf{k}, j\}$, numbering all the branches of phonon modes and all the values of the wave vector $\mathbf{k}$ in the first Brillouin zone, and $a_{æ}(\mu\Gamma\gamma)$ are the so–called Van–Vleck coefficients which are linear combinations of the eigenvectors $w_\alpha(æ)$ of the dynamic matrix. The projected densities of phonon states can be introduced as the image parts of the corresponding Green's functions:

$$\rho_\Gamma^{(0)}(\mu\lambda;\ \omega) = -2\mathrm{Im} D_\Gamma^{(0)}(\mu\lambda;\ \omega + i\epsilon)_{\epsilon=+0},$$

where

$$D_\Gamma^{(0)}(\mu\lambda) = \langle\langle Q_{\mu\Gamma\gamma} \mid Q_{\lambda\Gamma\gamma} \rangle\rangle.$$

If the dynamic matrix is diagonal, the Green's functions $D_\Gamma^{(0)}(\mu\lambda)$ can be easily expressed in terms of the Van–Vleck coefficients and the phonon frequencies:

$$D_\Gamma^{(0)}(\mu\lambda) = \frac{1}{2\pi} \sum_{æ} \frac{a_{æ}(\mu\Gamma\gamma) a^*_{æ}(\lambda\Gamma\gamma)}{\omega^2 - \omega_{æ}^2}. \qquad (2)$$

Fig. 3 presents the projected densities of phonon states obtained for the ideal host crystal CdTe by the RIM–11 for different Γ present in the decomposition of the Γ_{tot}. As seen from the figures the densities of vibrations have characteristic peaks and maxima in the regions of acoustical and optical phonon bands, their frequency position and peak intensity depending on the type of symmetry of the projected density.

The perturbation of the dynamic matrix coming from doping results in an essential redistribution of the projected phonon spectral density. Fig. 4 and 5 present the projected densities corresponding to symmetrized phonons of $A_1, E, T_2^{(a)}$ and $T_2^{(b)}$ types taken for the positive value of the defect parameter t, $t = 0.30$. This means that the force constant f in the impurity complex is somewhat smaller than in the pure host crystal. As follows from our calculations the projected densities change with the increasing of the force constant f so that their maximum becomes more acute and shifts towards the low–frequency region of the spectrum. Analogous changes take place with increasing of f in the case of negative values of t, i.e. when the impurity force constant is somewhat larger than the host crystal one. These changes of the projected phonon densities of the A_1 and T_2 types indicate a tendency to form resonant phonon modes of the A_1 and T_2 types with doping. At the same time the projected phonon densities of the E types do not undergo significant changes at physically reasonable values of the parameter t.

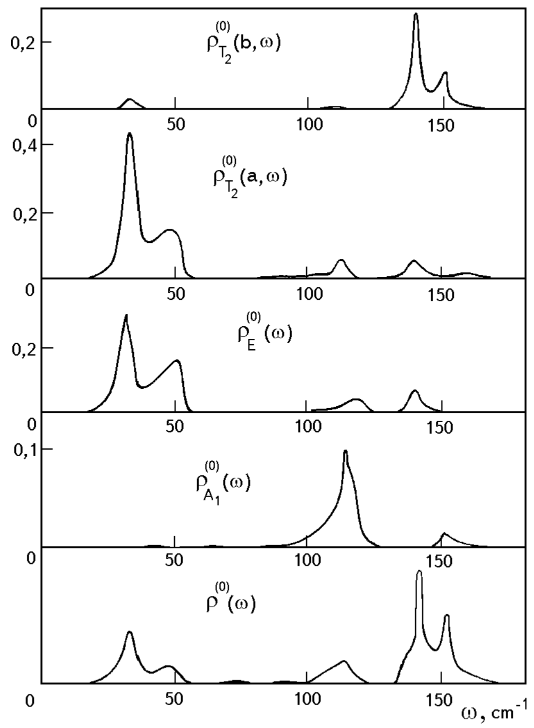

Fig. 3. Projected densities of the phonon states of the pure host lattice of CdTe for symmetrized displacements of different symmetry.

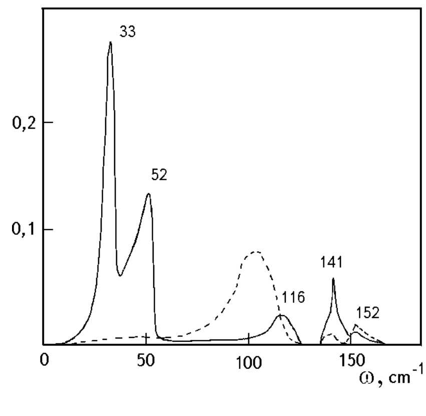

Fig. 4. Projected densities of the phonon states of E (full line) and A_1 (broken line) types for CdTe doped by Co^{2+} with the defect of force constants taken into account ($t = 0.30$).

It is of special interest to compare the experimentally observed band of optical absorption $^4A_2 \to {}^4T_1$ in the impurity system CdTe:Co^{2+} with the results of the classical theory of impurity absorption of light [10] which does not take into consideration the Jahn–Teller and/or other non–adiabatic effects. As seen from fig. 2 the optical band of the $^4A_2 \to {}^4T_1$ transition occupies the spectral range from 11769 cm^{-1} to 12070 cm^{-1}, i. e. it possesses the width of about 300 cm^{-1}. Taking into consideration that the maximal phonon frequency in the crystal lattice of CdTe is about 167 cm^{-1}, we can conclude that the optical band in question presents the case of a weak–to–intermediate electron–phonon coupling when the major contribution to optical band comes from the zero–phonon line and its one–phonon and two–phonon satellites.

Thus all the complicated fine structure of the optical band $^4A_2 \to {}^4T_1$ observed in the spectral range from 11769 cm^{-1} to 11987 cm^{-1} should be attributed to the one–phonon and two–phonon satellites. What concerns the latter one it should be much less intensive as compared with the one–phonon side–band in the limiting case of weak coupling and moreover it is placed in the spectral range which is shifted somewhat more towards high frequencies than the one–phonon satellite. Therefore, it is reasonable to assume that the intensive spectral lines observed at 42 cm^{-1}, 65 cm^{-1}, 102 cm^{-1}, 136 cm^{-1}, 159 cm^{-1} in the high–frequency side from the zero–phonon line in the optical band $^4A_2 \to {}^4T_1$ belong to the one–phonon satellite.

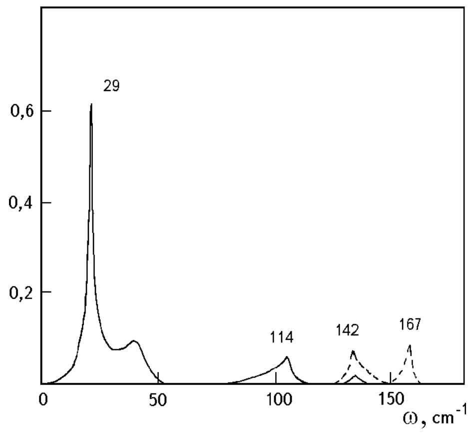

Fig. 5. Projected densities of the phonon states of $T_2^{(a)}$ (full line) and $T_2^{(b)}$ (broken line) types for CdTe doped by Co^{2+} with the defect of force constants taken into account ($t = 0.30$).

As is generally known (e. g. [10]) the coefficient of impurity optical absorption of light with the participation of one phonon of crystal lattice vibrations at $T = 0$ K in the model of small radius impurity center can be written as

$$K^{(1)}(\omega) = \text{const} \sum_{\Gamma} [\Gamma]\ V_\Gamma^2\ \rho_\Gamma^{(0)}(\omega), \tag{3}$$

where Γ is irreducible representation, the vibrations active in the optical transition in question belong to, $[\Gamma]$ is a dimension of the representation Γ, V_Γ is the corresponding constant of linear electron–phonon coupling, and $\rho_\Gamma^{(0)}(\omega)$ is projected density of phonons transforming as Γ. The frequency ω is counted off from the zero–phonon line, $\omega = \Omega - [E(\Gamma_8^{(\psi)}) - E(\Gamma_8)]/\hbar$, where Ω is the frequency of absorbed light. Comparing the one–phonon side–band in question with the projected phonon densities of the $A_1, E, T_2^{(a)}$ and $T_2^{(b)}$ types active in the optical transition under consideration and shown in fig. 3–5 we come to the conclusion that the observed fine structure of the absorption band $^4A_2 \to {}^4T_1$ cannot be explained in terms of the classical theory ignoring the Jahn–Teller effect in the excited electronic term $\Gamma_8^{(\psi)}(^4T_1)$.

The projected densities of phonon states of the pure host crystal shown in fig. 3 do not have maxima and resonant peaks at the frequencies listed above. Moreover doping the Co^{2+} ions into the crystal of CdTe results in an insufficient (from this point of view) redistribution of the phonon densities. The maximum of the projected density of the A_1 type can be matched with the observed spectral line at 102 cm^{-1} if the impurity complex force constant f is taken 30 % less than the pure crystal one. However the peaks of the other phonon densities do not reach this spectral range at any physically reasonable value of the defect parameter t. In particular, at the value of t corresponding to the 30 % decrease of the impurity complex force constant the spectral lines at 42 cm^{-1} and 65 cm^{-1} do not fit any of the maxima of the low–symmetry phonon densities of the A_1, E, $T_2^{(a)}$ and $T_2^{(b)}$ types.

IV. THE MULTIMODE JAHN–TELLER EFFECT $\Gamma_8 \bigotimes (E + T_2)$ IN THE ONE–PHONON SIDE–BAND OF THE OPTICAL ABSORPTION SPECTRUM $\Gamma_8(^4A_2) \to \Gamma_8{}^{(\psi)}(^4T_1)$

Theoretical analysis of fine vibronic structure of the optical absorption band in the frequency interval 11769 cm^{-1}–11987 cm^{-1} corresponding to the transition $\Gamma_8(^4A_2) \to \Gamma_8^{(\psi)}(^4T_1)$ can be performed under the following two simplifying assumptions.

(i) The Jahn–Teller effect in the ground electronic term $\Gamma_8(^4A_2)$ the optical transition occurs from can be neglected. The wave function of the ground electron–vibrational state of the term $\Gamma_8(^4A_2)$ then can be written in the multiplicative form $|\,\Gamma_8\gamma\rangle = |0\rangle|\Gamma_8(^4A_2),\gamma\rangle$ where $|0\rangle$ denotes the ground vibrational state of the impurity crystal lattice, the phonon vacuum, and $|\Gamma_8(^4A_2),\gamma\rangle$ is the electronic wave function transforming as the γth line of the irreducible representation Γ_8 of the T_d symmetry group.

(ii) The Jahn–Teller effect in the excited electronic term $\Gamma_8^{(\psi)}(^4T_1)$ the optical transition occurs to can be considered so weak that the perturbation theory approach with respect to the vibronic coupling constants is applicable. Though as mentioned in the previous section the two–phonon side–band is also observed in the optical band under consideration and therefore the electron–phonon coupling for this band should be treated as weak–to–intermediate we believe the perturbative weak–coupling approach gives reasonable results at least in what concerns the tendencies of appearance of new resonant and local vibronic states.

Vibronic Hamiltonian for multimode Jahn–Teller effect of the $\Gamma_8 \bigotimes (e+t_2)$ type for an impurity center of small radius can be written in the form [2]:

$$H = H_0 + V,$$

where

$$H_0 = \frac{1}{2}\sum_{æ}(P_{æ}^2 + \omega_{æ}^2 Q_{æ}^2);$$

$$V = \sum V_{\mu\Gamma} Q_{\mu\Gamma\gamma} \hat{C}_{\Gamma\gamma}. \qquad (4)$$

Here H_0 is Hamiltonian of free vibrations of the impurity crystal lattice, including already the effects resulting from the defects of mass and of force constants (section III). The second expression in (4) describes linear vibronic coupling of the impurity electronic states $\mid \Gamma_8^{(\psi)}(^4T_1), \gamma\rangle$ to symmetrized nuclear displacements $Q_{\mu\Gamma\gamma}$ of the nearest neighboring atoms. The indices Γ and γ denote irreducible representations and their rows the symmetrized displacements active in the Jahn–Teller effect transform as. In our case $\{\Gamma_8^2\} = A_1 + E + T_2$ and therefore Γ in (4) equals E and T_2, the coupling to the A_1 modes being trivial and separated. Hence the Jahn–Teller effect $\Gamma_8 \bigotimes (e+t_2)$ case should be considered. Note that the vibrational impurity cluster $CoTe_4$ including atoms of the first coordination sphere contain two irreducible representations T_2. This means that among nine vibrational degrees of freedom this cluster possesses two sets of symmetrized nuclear displacements of the T_2 type, $\{Q_{aT_2}\}$ and $\{Q_{bT_2}\}$, μ in (4) runs over these two sets, $\mu = a, b$ for $\Gamma = T_2$. Note also that the symmetrized nuclear displacements $Q_{\mu\Gamma\gamma}$ are not normal coordinates but their linear combination (1). Therefore the model of small radius impurity center Hamiltonian (4) is based upon does not reduce to the cluster model. The coefficients $V_{\mu\Gamma}$ in (4) are constants of linear vibronic coupling, whereas the matrices $\hat{C}_{\Gamma\gamma}$ are composed from the corresponding Clebsch–Gordan coefficients and are determined in the space spanned over the degenerate electronic states $\mid \Gamma_8^{(\psi)}(^4T_1), \gamma\rangle$ of the excited term $\Gamma_8^{(\psi)}(^4T_1)$. In our case they can be written in the form

$$\hat{C}_\theta = \begin{pmatrix} 1 & 0 & 0 & 0 \\ 0 & -1 & 0 & 0 \\ 0 & 0 & -1 & 0 \\ 0 & 0 & 0 & 1 \end{pmatrix}, \hat{C}_\epsilon = \begin{pmatrix} 0 & 0 & 1 & 0 \\ 0 & 0 & 0 & 1 \\ 1 & 0 & 0 & 0 \\ 0 & 1 & 0 & 0 \end{pmatrix},$$

$$\hat{C}_\xi = \begin{pmatrix} 0 & i & 0 & 0 \\ -i & 0 & 0 & 0 \\ 0 & 0 & 0 & -i \\ 0 & 0 & i & 0 \end{pmatrix}, \qquad (5)$$

$$\hat{C}_\eta = \begin{pmatrix} 0 & 1 & 0 & 0 \\ 1 & 0 & 0 & 0 \\ 0 & 0 & 0 & 1 \\ 0 & 0 & 1 & 0 \end{pmatrix}, \hat{C}_\zeta = \begin{pmatrix} 0 & 0 & -i & 0 \\ 0 & 0 & 0 & -i \\ i & 0 & 0 & 0 \\ 0 & i & 0 & 0 \end{pmatrix},$$

where θ and ϵ denote lines of the E representation, and ξ, η and ζ serve for T_2.

In the absence of vibronic coupling the electron–vibrational states of the impurity–phonon system are characterized by the number of phonons. Thus, the one–phonon states can be obtained by acting the operators of creation one phonon $b_{æ}^{+} = -i(P_{æ} + i\omega_{æ} Q_{æ})/\sqrt{2\hbar_{æ}\omega_{æ}}$ over the phonon vacuum state $\mid 0\rangle$. Their contribution in optical absorption is determined by the coefficient $a_{æ}(\mu\Gamma\gamma)$ the corresponding normal mode $Q_{æ}$ participates in accordance to (1). Therefore we follow [11] and introduce symmetrized operators of creation,

$$b_{\alpha\Gamma\gamma}^{+}(\omega) = N_\Gamma \sum_{æ} a_{æ}(\alpha\Gamma\gamma)\delta(\omega - \omega_{æ}) b_{æ}^{+}, \qquad (6)$$

where N_Γ is the normalization factor which can be obtained from the commutation relations,

$$[b_{\alpha\Gamma\gamma}(\omega), b_{\beta\bar{\Gamma}\bar{\gamma}}(\omega')] = \delta_{\alpha\beta}\delta_{\Gamma\bar{\Gamma}}\delta_{\gamma\bar{\gamma}}\delta(\omega - \omega'). \qquad (7)$$

The classic theory of one–phonon side–bands has been developed for nondegenerate electronic states. Its generalization to the case of orbital degeneracy, when the Jahn–Teller effect occurs in the excited electronic term participating in the optical transition is not trivial. First, when the vibronic interaction is considered the phonon occupation numbers of the Jahn–Teller–active normal vibrations cease to be good quantum numbers and the vibronic states of the Jahn–Teller impurity center are no longer characterized by a definite value of the phonon numbers. From this point of view the "one–phonon side–band" corresponding to optical transitions, for which the "vibrational state" of the Jahn–Teller impurity center change by a unit, have no meaning. Secondly, the vibronic energy levels are not equally spaced [2] and therefore the coincidence of the energies of the allowed transitions, and thus the corresponding superposition of the spectral lines forming the "zero–phonon" line, the "one–phonon" satellite, etc. is extremely improbable.

However in the case of sufficiently enough vibronic coupling when the latter can be handled by perturbation theory in the first nonvanishing order the number of phonons still remains a good quantum number. In this sense we can consider one–phonon vibronic state of the Jahn–Teller system and their contribution in the one–phonon side–band of the $\Gamma_8(^4A_2) \rightarrow \Gamma_8^{(\psi)}(^4T_1)$ transition. The zeroth–order symmetry adapted wave function composed from the one–phonon states can be written in the Clebsch–Gordan convolution form:

$$\mid \Gamma\gamma\rangle_\omega = \sum_{\alpha\Gamma_1\gamma_1}\sum_{\gamma_2}\langle\Gamma_1\gamma_1\ \Gamma_8\gamma_2 \mid \Gamma\gamma\rangle b^+_{\alpha\Gamma_1\gamma_1}(\omega) \mid 0\rangle \mid \Gamma_8(^4A_2),\gamma_2\rangle, \tag{8}$$

where $\langle\Gamma_1\gamma_1\ \Gamma_8\gamma_2 \mid \Gamma\gamma\rangle$ are the Clebsch–Gordan coefficients of the symmetry group T_d.

To obtain the one–phonon vibronic wave function in the first order perturbation theory we use the operator version of perturbation theory. The Jahn–Teller Hamiltonian can be diagonalized by the unitary transformation $\hat{U} = \exp(-i\hat{S})$ where the operator $\hat{S}$ in the first order of perturbation theory obeys the operator equation $[\hat{S}, H_0] = iV$ [2]. Substituting H_0 and V from (4) we find

$$\hat{S} = -\frac{1}{\hbar}\sum_{\alpha\Gamma\gamma}\sum_{æ} V_{\alpha\Gamma}\omega_{æ}^{-2}a_{æ}(\alpha\Gamma\gamma)\hat{C}(\Gamma\gamma)P_{æ}. \tag{9}$$

Presenting $\exp(-i\hat{S})$ at small $V_{\alpha\Gamma}$ as $1 - i\hat{S}$ and acting with this operator over the zero–order symmetry adapted one–phonon wave function (8) we come to the one–phonon vibronic states in the first order of perturbation theory,

$$\mid \Gamma\gamma\}_\omega = \mid \Gamma\gamma\rangle_\omega - i\hat{S} \mid \Gamma\gamma\rangle_\omega. \tag{10}$$

Spectral density of the one–phonon side–band is determined by the following expression:

$$K^{(1)}(\Omega) = \int d\omega \sum_{\gamma}\sum_{\bar{\Gamma}\bar{\gamma}} \mid \{\Gamma_8(^4A_2),\gamma \mid d \mid \bar{\Gamma}\bar{\gamma}\}_\omega \mid^2 \delta(\Omega - \Omega_0 - \omega). \tag{11}$$

Here $d = e\mathbf{ED}$ is operator causing the electric dipole optical transition, $\mathbf{E}$ is the amplitude value of the electric field of the absorbed electromagnetic wave, $\mathbf{D}$ is dipole moment of impurity electrons, and $\Omega_0 = [E(\Gamma_8^{(\psi)}(^4T_1)) - E(\Gamma_8(^4A_2))]/\hbar$ is frequency of electron transition in the impurity system. Substituting into (11) the states $\mid \Gamma_8(^4A_2)\gamma\}$ taken in the multiplicative form $\mid 0\rangle \mid \Gamma_8(^4A_2),\gamma\rangle$ and the states $\mid \bar{\Gamma}\bar{\gamma}\}_\omega$ in the form (10), presenting the δ–function in its Fourier integral form, putting the time–frequency exponent $\exp(-it(\Omega - \Omega_0 - \omega))$ in the matrix element, using the fact that $\exp(-i\omega t) \mid \bar{\Gamma}\bar{\gamma}\}_\omega \approx \exp(iH_0t/\hbar)\exp(-iHt/\hbar) \mid \bar{\Gamma}\bar{\gamma}\}_\omega$, and reducing the sum over the intermediate indexes ω and $\bar{\Gamma}\bar{\gamma}$ we get

$$K^{(1)}(\Omega) = \frac{I_0}{\hbar^2\omega^2}\sum_{\Gamma_1\gamma_1}\sum_{\Gamma_2\gamma_2}\sum_{\mu\lambda}\langle\gamma \mid \hat{C}_{\Gamma_1\gamma_1} \mid \mu\rangle\langle\lambda \mid \hat{C}_{\Gamma_2\gamma_2} \mid \gamma\rangle$$

$$\sum_{\alpha\beta} V_{\alpha\Gamma_1}V_{\beta\Gamma_2}\langle\mu \mid \langle 0 \mid Q_{\alpha\Gamma_1\gamma_1}; Q_{\beta\Gamma_2\gamma_2} \mid 0\rangle_\omega \mid \lambda\rangle \mid \omega = \Omega - \Omega_0. \tag{12}$$

Here we simplified the notation used, $\mid \gamma\rangle = \mid \Gamma_8^{(\psi)}(^4T_1),\gamma\rangle$, $\mid \mu\rangle = \mid \Gamma_8^{(\psi)}(^4T_1),\mu\rangle$, $\mid \lambda\rangle = \mid \Gamma_8^{(\psi)}(^4T_1),\lambda\rangle$, and $\langle\mu \mid \langle 0 \mid Q_{\alpha\Gamma_1\gamma_1} : Q_{\beta\Gamma_2\gamma_2} \mid 0\rangle_\omega \mid \lambda\rangle$ is the $\mu\lambda$ matrix element of Fourier transform of matrix correlation function,

$$\langle 0 \mid Q_{\alpha\Gamma_1\gamma_1}; Q_{\beta\Gamma_2\gamma_2} \mid 0\rangle_\omega = \frac{1}{2\pi}\int_{-\infty}^{\infty} e^{i\omega t}\langle 0 \mid Q_{\alpha\Gamma_1\gamma_1}(t)Q_{\beta\Gamma_2\gamma_2} \mid 0\rangle dt. \tag{13}$$

The factor I_0 in (12) corrects for square of modules of the transition matrix element determining integral intensity of the optical band,

$$I_0 = \sum_{\gamma_1\gamma_2} \mid \langle\Gamma_8(^4A_2),\gamma_1 \mid d \mid \Gamma_8^{(\psi)}(^4T_1),\gamma_2\rangle \mid^2 .$$

The correlation function (13) is related with the image part of the corresponding matrix Green's function, [2]

$$\langle 0 \mid Q_{\alpha\Gamma_1\gamma_1}; Q_{\beta\Gamma_2\gamma_2} \mid 0\rangle_\omega = -2\hbar\theta(\omega)\mathrm{Im}\langle\langle Q_{\alpha\Gamma_1\gamma_1} \mid Q_{\beta\Gamma_2\gamma_2}\rangle\rangle_{\omega+i\epsilon}, \tag{14}$$

where $\epsilon = +0$ and $\langle\langle Q_{\alpha\Gamma_1\gamma_1} \mid Q_{\beta\Gamma_2\gamma_2}\rangle\rangle\omega$ is Fourier transform of the retarded matrix Green's function,

$$\langle\langle Q_{\alpha\Gamma_1\gamma_1} \mid Q_{\beta\Gamma_2\gamma_2}\rangle\rangle_t$$
$$= -\frac{i}{\hbar}\theta(t)\langle 0 \mid [Q_{\alpha\Gamma_1\gamma_1}(t), Q_{\beta\Gamma_2\gamma_2}] \mid 0\rangle. \quad (15)$$

The problem of the multimode Jahn–Teller effect $\Gamma_8 \bigotimes (e + t_2)$ in the weak coupling case has been solved by Vaisleib *et al.* [11,12]. This allows to omit the details of the corresponding perturbative approach. The only thing to emphasize is that for the phonon matrix Green's function (15) used in the present paper the result can be easily obtained by the following decoupling just in the second equation of the infinite system of equations of motion,

$$\langle\langle[\hat{C}_{\Gamma_1\gamma_1}, \hat{C}_{\Gamma_2\gamma_2}]Q_{\alpha\Gamma\gamma} \mid Q_{\beta\bar{\Gamma}\bar{\gamma}}\rangle\rangle$$
$$\cong [\hat{C}_{\Gamma_1\gamma_1}, \hat{C}_{\Gamma_2\gamma_2}]\langle\langle Q_{\alpha\Gamma\gamma} \mid Q_{\beta\bar{\Gamma}\bar{\gamma}}\rangle\rangle,$$

closing the chain of equations. Finally we come to the following result. Spectral density of the one–phonon side–band (12) is additive with respect to irreducible representations labeling the symmetrized nuclear displacements $Q_{\mu\Gamma\gamma}$ linearly coupled to the $\Gamma_8^{(\psi)}(^4T_1)$ term under consideration,

$$K^{(1)}(\Omega) = K^{(1)}_{A_1}(\Omega) + K^{(1)}_E(\Omega) + K^{(1)}_{T_2}(\Omega). \quad (16)$$

Each term in (16) describes the corresponding contribution in the one–phonon side–band coming from the nuclear displacements of the appropriate symmetry. The term $K^{(1)}_{A_1}$ coincides with the known result of the classical theory of singlet–singlet transitions (cf. with (3)):

$$K^{(1)}_{A_1}(\Omega) = \frac{I_0 V_A^2}{\hbar\omega^2}\theta(\omega)\rho^{(0)}_{A_1}(\omega) \mid_{\omega=\Omega-\Omega_0} . \quad (17)$$

For the $K^{(1)}_E$ term we find

$$K^{(1)}_E(\Omega)$$
$$= 2\sqrt{2}\frac{\hbar}{\pi}I_0\frac{\theta(\omega)\gamma_E(\omega)}{[\hbar\omega + 2\pi V_E^2 r^{(0)}_E(\omega)]^2 + \gamma^2_E(\omega)}\Big|_{\omega=\Omega-\Omega_0}, \quad (18)$$

where

$$\gamma_E(\omega) = 2\pi V_E^2\rho^{(0)}_E(\omega) \quad (19)$$

and

$$r^{(0)}_\Gamma(\omega) = -\frac{1}{\pi}\int_0^\infty \frac{2z\rho^{(0)}_\Gamma(z)}{\omega^2 - z^2}dz. \quad (20)$$

For the term $K^{(1)}_{T_2}$ we have:

$$K^{(1)}_{T_2}(\Omega)$$
$$= \frac{3\hbar}{4\pi}I_0\frac{\gamma_{T_2}(\omega)}{[\hbar\omega + 4\pi r^{(0)}_{T_2}(\omega)]^2 + \gamma^2_{T_2}(\omega)}\Big|_{\omega=\Omega-\Omega_0}, \quad (21)$$

where

$$\gamma_{T_2}(\omega) = 4\pi\rho^{(0)}_{T_2}(\omega);$$
$$\rho^{(0)}_{T_2}(\omega) = \sum_{\alpha\beta} V_{\alpha T_2}V_{\beta T_2}\rho^{(0)}_{T_2}(\alpha\beta, \omega),$$

and $r^{(0)}_{T_2}$ is given in (20) with $\Gamma = T_2$ whereas $\rho^{(0)}_{T_2}(\alpha\beta, \omega)$ is given by expression (2).

As follows from these results the spectral densities of the partial contributions in the one–phonon satellite $K^{(1)}_\Gamma$ resulting from the Jahn–Teller active vibrations of the E and T_2 type are essentially different as compared with the starting phonon densities $\rho^{(0)}_E$ and $\rho^{(0)}_{T_2}$. The corresponding expressions are of the resonant type. This means that the most important redistribution of the starting phonon density occurs at spectral regions close to roots (if any) of the transcendental equations

$$\hbar\omega + 2\pi V_E^2 r^{(0)}_E(\omega) = 0,$$
$$\hbar\omega + 4\pi r^{(0)}_{T_2}(\omega) = 0,$$

where the denominators in (18) and (21) are minimal, the peak intensity of the corresponding resonances being the larger the less is the background spectral density $\rho^{(0)}_E$ or $\rho^{(0)}_{T_2}$ in this spectral region.

Fig. 6 and 7 present partial spectral densities of the one–phonon side–band $K^{(1)}_E$ and $K^{(1)}_{T_2}$ at different values of linear vibronic coupling constants. It is seen that they are significantly different from the starting densities of phonon states $\rho^{(0)}_E(\omega)$ and $\rho^{(0)}_{T_2}(\alpha\beta, \omega)$ and, particularly, the resonances (their spectral position and intensity) depend essentially on the values of the vibronic coupling constants.

V. DISCUSSION

In the experimentally observed optical absorption spectrum of the $\Gamma_8(^4A_2) \to \Gamma_8^{(\psi)}(^4T_1)$ transition in the one–phonon spectral region one can distinguish the following three intervals. The first one, from 0 to 85 cm^{-1}

possesses two peaks of absorption, at 42 cm^{-1} and 65 cm^{-1}. The second one, from 85 cm^{-1} to 125 cm^{-1} has a maximum at 102 cm^{-1} and the third one, from 125 cm^{-1} to 170 cm^{-1} possesses two peaks of weak intensity. Each of these intervals can be attributed to the transverse and longitudinal, acoustical and optical vibrations of the crystal lattice in the projected phonon densities respectively. For instance, the peak at 102 cm^{-1} can be assigned to the A_1 vibrations if we assume a reduction of force constants by about 30 %, $t = (f - f')/f = 0.30$. This estimate results from the following considerations.

(a) As comes from the calculated phonon densities (fig. 3) only the A_1 vibrations have a considerably strong spectral density in the low–frequency region of acoustical phonons. The maximum of this density of states is at 114 cm^{-1} in the case of pure host crystal.

(b) Only for the A_1 vibrations this maximum shifts towards the low–frequency spectral region with the force constants changed, its position becoming equal to the experimental frequency 102 cm^{-1} at $t = 0.30$.

(c) The peak at 102 cm^{-1} cannot be explained by a contribution of the E or T_2 vibrations with taking into account the effects of vibronic coupling because for such a fitting we need unrealistically large magnitudes of linear vibronic coupling constants.

Hence this consideration can be used as the reference procedure ascertaining the defect of force constants by doping of CdTe by Co^{+2} ions to be about 0.30. The projected densities of states with this value of force constants taken into account are shown in fig. 4 and 5. The phonon density of the E type remains practically unchanged as compared with its form for the pure host crystal case and it has peaks at the frequencies 33 cm^{-1}, 52 cm^{-1}, 116 cm^{-1}, 141 cm^{-1} and 152 cm^{-1}. Densities of $T_2^{(a)}$ and $T_2^{(b)}$ vibrations become somewhat redistributed, they possess peaks at 29 cm^{-1}, 114 cm^{-1}, 142 cm^{-1} and 167 cm^{-1}.

At the first step we include the Jahn–Teller effect for the E and T_2 vibrations separately. Consider effects of vibronic coupling to E modes, i. e. let $V_{T_2}^{(a)} = V_{T_2}^{(b)} = 0$. As seen from fig. 6 the vibronic coupling being included the two peaks, at 33 cm^{-1} and 52 cm^{-1}, shift towards the high–frequency region, and with increasing the V_E constant they draw nearer to the experimentally observed positions. Besides, one can see a redistribution of intensities of these two peaks also nearer to the experimental data. In fig. 8 the energy positions of these two peaks are plotted versus the vibronic constant V_E. The broken lines show the maximum positions of the projected density of states redetermined by the Jahn–Teller effect, whereas a full line corresponds to the resonant states of vibronic origin arising at the frequency region beginning from 55 cm^{-1} where the background density of states is low enough. At V_E=70 cm^{-1}/Å(a.u.m.)$^{-1/2}$ the energy position of this state merges with the experimental frequency 65 cm^{-1}. Another less intensive peak in the calculated spectral density in this case is at 39 cm^{-1} that is close enough to the experimental value of 42 cm^{-1}.

The one–phonon side–band calculated with the vibronic coupling constants V_E = 70 cm^{-1}/Å(a.u.m.)$^{-1/2}$

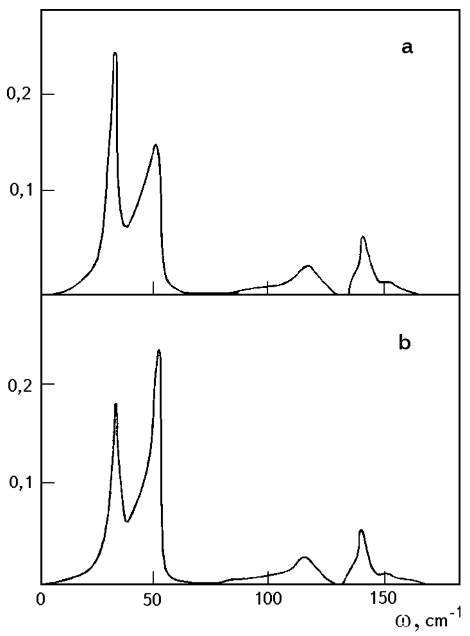

Fig. 6. Partial contribution in the one–phonon side–band $K_E^{(1)}$ resulting from the multimode Jahn–Teller effect with taking into account vibronic coupling to E modes at different values of vibronic constant (a — $V_E = 2$ cm^{-1}/Å(a.u.m.)$^{-1/2}$, b — V_E =10 cm^{-1}/Å(a.u.m.)$^{-1/2}$).

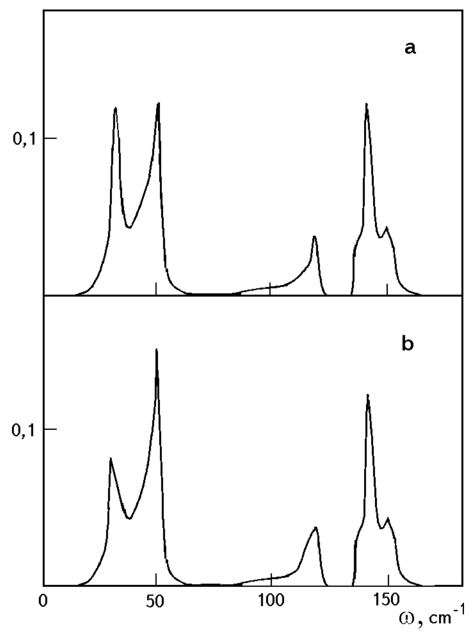

Fig. 7. Partial contribution in the one–phonon side–band $K_{T2}^{(1)}$ resulting from the multimode Jahn–Teller effect with taking into account vibronic coupling to T_2 modes at different values of the dimensionless vibronic constant (a — $V_{T_2}^{(a)} = V_{T_2}^{(b)} = 5$ cm^{-1}/Å(a.u.m.)$^{-1/2}$, b — $V_{T_2}^{(a)} = V_{T_2}^{(b)} = 10$ cm^{-1}/Å(a.u.m.)$^{-1/2}$).

and $V_{A_1} = 50$ cm^{-1}/Å(a.u.m.)$^{-1/2}$ is presented in fig. 9. The value of V_{A_1} has been taken so that the peak at 102 cm^{-1} has equal intensity with the peak at 39 cm^{-1} resulting from E vibrations. Then the intensity of the 102 cm^{-1} peak has been fitted with the experimentally observed one.

From the above consideration of the effects of vibronic coupling to E modes only one can deduce the following conclusions correct for the case of vibronic coupling to T_2 modes as well.

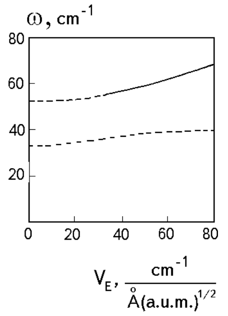

Fig. 8. The energy positions (dashed lines) of low frequency peaks in the one–phonon side–band versus linear vibronic coupling constant. The solid line corresponds to resonant states of the vibronic origin.

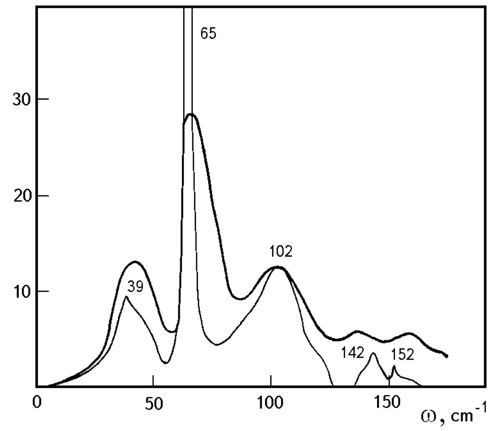

Fig. 9. The vibronic structure of the one–phonon side–band in the low–frequency region adjacent to zero–phonon line of the optical absorption Γ_8 $(^4A_2) \to \Gamma_8^{(\psi)}$ $(^4T_1)$ in the impurity system CdTe:Co^{2+}. The thick line presents experiment, the thin line: theoretical results corresponding to (16)–(21) at $V_{A_1} = 50$ cm^{-1}Å(a.u.m.)$^{-1/2}$; V_E=70 cm^{-1}Å(a.u.m.)$^{-1/2}$; $V_{T_2}^{(a)} = V_{T_2}^{(b)} = 0$.

(a) The Jahn–Teller effect plays a determining role in the low–frequency region of absorption spectrum close to zero–phonon line and does not affect the high frequency spectral region above 85 cm^{-1}. This conclusion follows from the factor $1/\hbar\omega$ in the denominator $1-(4\pi V_\Gamma^2/\hbar\omega)D_\Gamma^{(0)}(\omega)$ of the expression for Green's functions.

(b) Fine structure of the one–phonon side–band in the two remaining spectral intervals is determined mainly by local vibrational dynamics of the crystal lattice, the Jahn–Teller effect resulting in a slight change peak intensities only. Moreover, in the spectral interval from 85 cm^{-1} to 125 cm^{-1} the form of the spectral line is caused by the interaction with the A_1 vibrations and in the optical phonon region other types of vibrations contribute as well.

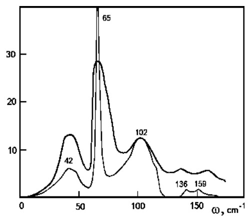

Fig. 10. The vibronic structure of the one–phonon side–band in the low–frequency region adjacent to the zero–phonon line of the optical absorption Γ_8 $(^4A_2) \to \Gamma_8^{(\psi)}$ $(^4T_1)$ in the impurity system CdTe:Co^{2+}. The thick line presents the experiment, the thin line: theoretical results corresponding to (16)–(21) at $V_{A_1} = 120$ cm^{-1}Å(a.u.m.)$^{-1/2}$; $V_E = 0$; $V_{T_2}^{(a)} =$ 60 cm^{-1}Å(a.u.m.)$^{-1/2}$, $V_{T_2}^{(b)} = 34$ cm^{-1}Å(a.u.m.)$^{-1/2}$.

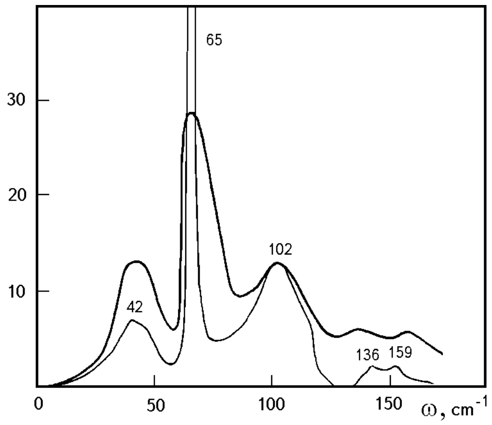

Fig. 11. The vibronic structure of the one–phonon side–band in the low–frequency region adjacent to the zero–phonon line of the optical absorption $\Gamma_8(^4A_2) \to \Gamma_8^{(\psi)}(^4T_1)$ in the impurity system CdTe:Co^{2+}. The thick line presents the experiment, the thin line: theoretical results corresponding to (16)–(21) at $V_{A_1} = 120$ cm^{-1}Å(a.u.m.)$^{-1/2}$; $V_E = 70$ cm^{-1} Å (a.u.m.)$^{-1/2}$; $V_{T_2}^{(a)} = 60$ cm^{-1}Å(a.u.m.)$^{-1/2}$, $V_{T_2}^{(b)} = 34$ cm^{-1}Å(a.u.m.)$^{-1/2}$.

We shall consider now the effects of vibronic coupling to T_2 vibrations with the coupling to E vibrations neglected ($V_E = 0$). General tendencies in this case are the same as in the previous case. However their analysis is more complicated because we have here two free parameters, the two vibronic constants $V_{T_2}^{(a)}$ and $V_{T_2}^{(b)}$. As in the E–mode case, the two peaks shift towards the high–frequency spectral region and their intensity is redistributed. At the frequencies above of 55 cm^{-1} a vibronic resonant state may occur but the same frequency position of this state can be obtained in different ways, with the different values of $V_{T_2}^{(a)}$ and $V_{T_2}^{(b)}$ i.e. there is an ambiguity of these coupling constants.

The form of the spectral line obtained under the assumption of vibronic coupling to A_1 and T_2 modes is given in fig. 10. The values of $V_{T_2}^{(a)} = 50\ \mathrm{cm}^{-1}/\text{Å}(\mathrm{a.u.m.})^{-1/2}$, $V_{T_2}^{(b)} = 34\ \mathrm{cm}^{-1}/\text{Å}(\mathrm{a.u.m.})^{-1/2}$ are taken as an example, however almost the same spectral line results from other sets of parameters giving the resonant state at 65 cm^{-1}. Simultaneous consideration of vibronic coupling to E and T_2 modes (fig. 11) does not give any new result if (as done before) the resonant line is fitted with the experimental position at 65 cm^{-1}.

Thus a satisfactory explanation of the experimental data can be obtained in the three cases presented in fig. 9–11. Two of them are obtained under the assumption of negligibly weak coupling to one of the two Jahn–Teller active types of vibration, E or T_2. Unfortunately we have no convincing arguments in favor of any of them.

Finally, we analyze in more detail the spectral density in the region from 125 cm^{-1} to 170 cm^{-1}. The high–frequency region of the experimental absorption spectrum possesses intensity of an order of magnitude less than in the low–frequency one and its fine structure is much less expressed. Only two spectral lines are observed, at 136 cm^{-1} and at 159 cm^{-1}. The calculated vibronic densities of states possess the same features, though they fit the experimental spectrum much worse.

As mentioned above the fine structure of the one–phonon absorption spectrum in the high–frequency region is determined mainly by the local vibrational dynamics of the crystal lattice. Among all the calculated projected densities for the pure host crystal only the T_2^b one possesses significant intensity in the spectral region of optical phonons. With the defect of mass (the case of impurity ions of Co^{2+}) taken into account this phonon density is redistributed and in particular its high frequency part is quenched. At $t = 0.30$ we obtain the high–frequency peaks at 142 cm^{-1} and 167 cm^{-1}. The A_1 modes give a peak at 152 cm^{-1} and the E modes give another one at 141 cm^{-1} (fig. 4 and 5). Taken together these phonon densities form the high–frequency wing of the one phonon spectrum presented in fig. 9–11. Thus the calculated line has peaks at 142 cm^{-1}, 152 cm^{-1} and 167 cm^{-1} their intensity being dependent on the corresponding vibronic constants. The energy position of the calculated peaks differs insufficiently from that of the experimentally observed spectral lines, however generally the envelope of this part of the one–phonon spectrum does not fit satisfactorily with the experiment.

One of the reasons for this lack of coincidence might be the two–phonon processes. The intensive spectral line observed experimentally at 199 cm^{-1} is one of the arguments in favor of this assumption. This line is placed at the frequency which is larger than the maximal phonon frequency of the pure CdTe and cannot come from the one–phonon satellite. Note that 199 cm^{-1} $\approx 2{\cdot}102$ cm^{-1} which means that the 102 cm^{-1} line seems to be a two–phonon replica of the 102 cm^{-1} line, the latter resulting from the non–Jahn–Teller A_1 mode.

VI. CONCLUSIONS

The optical band $\Gamma_8(^4A_2) \rightarrow \Gamma_8^{(\psi)}(^4T_1)$ of the impurity absorption of light in the CdTe:Co^{+2} system displays complicated fine structure in the low–frequency region adjacent to zero–phonon line. An attempt to attribute the observed spectral lines to maximum points of projected phonon densities of the defect crystal performed in section III in accordance with the classical theory has turned out to be unsuccessful in the case in question. This has been interpreted as resulting from inapplicability of the classical theory to cases when one of the electronic terms participating in optical transition possesses electron degeneracy and therefore is subject to the Jahn–Teller effect. To explain the complicated fine structure of the optical absorption band we have used the fact that the exited electronic term the electron transition occurs in comes from the $^4T_1$ term and therefore is coupled both to E and T_2 vibrations of crystal lattice. The results of the perturbation theory for the one–phonon side–band developed in section IV for the case under consideration can be satisfactorily fitted with the experimental data. Though the adjustment of the calculated spectrum to the experimental one needed to go somewhat beyond the limitations of the second–order perturbation theory satisfactory results demonstrate a certain flexibility of the calculated vibronic fine structure of the one–phonon side–band and its ability to fit the experimental curve at least in principle. We believe that this ability to reproduce tendencies of the vibronic spectra changes drastically the projected densities of states and in particular forms new resonant states which could not appear in the old classical theory ignoring the Jahn–Teller effect, and the case $\Gamma_8(^4A_2) \rightarrow \Gamma_8^{(\psi)}(^4T_1)$ can serve as a good example showing how the complex nature of coupled motion of impurity electrons and crystal lattice nuclei in Jahn–Teller system manifests itself in a complicated fine structure of one–phonon side–bands.

[1] G. Fisher, *Vibronic Coupling. The Interaction Between the Electronic and Nuclear Motions* (Academic Press, London, 1984).

[2] I. B. Bersuker, V. Z. Polinger, *Vibronic Interactions in Molecules and Crystals* (Springer Series in Chem. Phys., Berlin, Heidelberg, **49**, 1989).

[3] H. Koppel, W. Domcke, L. S. Cederbaum, Adv. Chem. Phys. **57**, 59 (1984).
[4] V. Z. Polinger, S. I. Boldyrev, Phys. Status Solidi B **137**, 241 (1984).
[5] A. I. Ryskin, A. L. Natadze, S. A. Kazanskiy, Zh. Eksp. Teor. Fiz. **64**, 910, (1973).
[6] A. L. Natadze, A. I. Ryskin, Izv. Acad. Nauk SSSR, Ser. Fiz. **140**, 1846 (1976).
[7] A. V. Vasil'ev, B. Z. Malkin, A. L. Natadze, A. I.Ryskin, Zh. Eksp. Teor. Fiz. **71**, 1192 (1976).
[8] K. Kunc, Ann. Phys. (Paris), **8**, 319 (1974).
[9] P. Plumelle, M. Vandevyver, Phys. Status Solidi B **73**, 271 (1976).
[10] A. A. Maradudin, *Theoretical and Experimental Aspects of the Effects of Point Defects and Disorder of the Vibrations of Crystals* (Academic Press, New York, 1966).
[11] A. V. Vaisleib, Yu. B. Rozenfel'd, V. P. Oleinikov, Fiz. Tverd. Tela **24**, 1074 (1982).
[12] A. V. Vaisleib, Yu. B. Rozenfel'd, V. P. Oleinikov, Phys. Lett. A **89**, 41 (1982).

БАГАТОМОДОВИЙ ЕФЕКТ ЯНА–ТЕЛЛЕРА В ОБЛАСТІ ОДНОФОНОННОЇ СМУГИ СПЕКТРУ ОПТИЧНОГО ПОГЛИНАННЯ $\Gamma_8(^4A_2e^4t^3) \to \Gamma_8^{(\psi)}(^4T_1e^3t^4)$ СИСТЕМИ CdTe:Co^{2+}

В. З. Полінгер[1], Ю. П. Гнатенко[1], Р. М. Буківський[1], С. В. Мельничук[2], І. М. Юрійчук[2]
[1] *Інститут фізики НАН України, Проспект Науки 46, Київ–28, Україна*
[2] *Чернівецький державний університет, вул. Коцюбинського, 2, Чернівці, 274012, Україна*

Теоретично і експериментально вивчена складна структура спектру низькотемпературного оптичного поглинання, зумовленого $d \to d$ переходами $\Gamma_8(^4A_2e^4t^3) \to \Gamma_8^{(\psi)}(^4T_1e^3t^4)$ в напівпровідниковому кристалі CdTe, леґованому Co^{2+}. Теоретична інтерпретація виконана з урахуванням багатомодового ефекту Яна–Теллера для збудженого $\Gamma_8^{(\psi)}(^4T_1e^3t^4)$ терму, що взаємодіє з тригональними і тетрагональними модами. Показано, що пояснити однофононну структуру спектру поглинання на основі класичної теорії без врахування ефекту Яна–Теллера неможливо. Структура однофононної смуги спектру оптичного поглинання суттєво відрізняється від структури зпроектованих густин станів, розрахованих для дефектного кристалу в моделі RIM–11. Багатомодовий ефект Яна–Теллера $\Gamma_8 \bigotimes (e + t_2)$ приводить (в другому порядку теорії збурень) до значного перерозподілу зпроектованих густин станів і появи нових резонансних вібронних мод. Експериментальний спектр поглинання в області однофононної смуги добре співпадає з теоретичною кривою, отриманою з відповідним набором вібронних констант.